Northumbria Research Link

1 **Holocene variability of East Asian summer monsoon as viewed from**

2 **the speleothem $\delta^{18}O$ records in central China**

3

4 Yanjun Cai[1,2,3], Xing Cheng[1,4], Le Ma[1], Ruixue Mao[1], Sebastian F.M. Breitenbach[5],

5 Haiwei Zhang[2], Gang Xue[1,4], Hai Cheng[2,6], R. Lawrence Edwards[6], Zhisheng An[1,3]

6

7 1. State Key Laboratory of Loess and Quaternary Geology, Institute of Earth

8   Environment, Chinese Academy of Science, Xi'an 710061, China

9 2. Institute of Global Environmental Change, Xi'an Jiaotong University, Xi'an

10   710049, China

11 3. Open Studio for OCCEC, Qingdao National Laboratory for Marine Science and

12   Technology, Qingdao, China

13 4. University of Chinese Academy of Sciences, Beijing 100049, China

14 5. Department of Geography and Environmental Sciences, Northumbria University,

15   NE1 8ST, United Kingdom

16 6. Department of Earth Sciences, University of Minnesota, Minneapolis, Minnesota

17   55455, USA

18

19 Corresponding Author: Yanjun Cai, yanjun_cai@xjtu.edu.cn

20

21 **Abstract**

22 Monsoon precipitation in East China shows distinct spatial distribution and its

23 variability is closely linked with the changes of the East Asian summer monsoon

24 (EASM). Located in the transition zone between the southern subtropical humid

25 climate and the northern warm temperate semi-humid climate, central China is a core

26 region for recognizing and understanding the spatio-temporal variability of the

27 EASM. Using U-series dating and stable isotope analysis on five stalagmites (MG-1,

28 MG-2, MG-7, MG-40 and MG-64) from Magou Cave, Henan Province, Central

29 China, we construct a high-resolution and precisely dated composite stalagmite $\delta^{18}O$

30 time series covering most of the Holocene. This composite record reveals variations

31 in precipitation $\delta^{18}O$ between 11.7 and 1.1 ka BP with average resolution of ~4 years.

32 The Magou composite record demonstrates that EASM intensity dominates long-term

33 changes in precipitation $\delta^{18}O$, which generally follows the northern hemisphere

34 summer insolation (NHSI) trend. Both, Ensemble Empirical Mode Decomposition

35 (EEMD) and wavelet filtering analyses real that the amplitudes of long-term (100-500

36 and 500-3000 years) components were slightly reduced between 8.5 and 4.9 ka BP,

37 implying a weakened influence of climatic forcings on centennial and even millennial

38 timescales during this warm period. Variance on 1-30-year timescales is relatively

39 low and ascribed to sampling resolution. Fourteen weak EASM intervals, including

40 the 8.2 ka event, were identified within the period corresponding broadly with the

41 Holocene Megathermal. Since no cold excursions other than the 8.2 ka event are

42 found in the Greenland ice core records, we tentatively propose that oscillations in

43 tropical sea surface temperature (SST) likely play an important role in steering other

44 weak monsoon events. Aligning the Magou composite record and other moisture

45 records with archaeological records from the study region, it seems that climate

46   change influenced both the spatial distribution and agricultural practices of ancient

47   cultures. However, overall moderate climatic changes in this region, most likely

48   characterized by shifts between subtropical humid climate and warm temperate semi-

49   humid climate, supported a generally consecutive development of ancient cultures

50   without major hiatuses.

51

1. Introduction

Increasing attention has been paid to the Holocene, the most recent geological chronozone, owing to close links of past climatic and environmental changes with the development of human civilizations, and the resemblance of the middle Holocene to future global climate conditions. In East Asia, numerous archives, including loess, lakes, peats, stalagmites, and sand-dune deposits have been used to study the history and variability of Holocene climate and environmental changes (An et al., 2000, 2012; Dykoski et al., 2005; Hong et al., 2003; Hu et al., 2008; Li et al., 2007; Wang et al., 2005; Xiao et al., 2004; Yang et al., 2019). Holocene temperature reconstructions from East Asia show generally consistent changes, i.e., relatively high temperatures during the early and middle Holocene, with the period of 8.5-3.3 ka called the Holocene Megathermal, and a subsequent gradual decrease throughout the late Holocene (Fang et al., 2011; Ge et al., 2007; Shi et al., 1992;), although some studies suggest a persistent temperature increase from the early to the late Holocene (Hou et al., 2019; Liu et al., 2014a;). However, precipitation (or effective precipitation) reconstructions show significant spatial variability. For example, already in 2000, An et al. (2000) proposed an asynchronous Holocene Optimum Period from north to south China, largely defined by the peak of effective precipitation. Subsequently, Ran and Feng (2013) proposed a gradual, lagged, increase of precipitation from south to north in eastern China. These studies largely focused on the characteristics of long-term changes throughout the Holocene, while few studies discussed climate events on centennial to decadal scales.

Detailed analysis of modern meteorological observations shows significant regional differences in monsoon precipitation across eastern China (Ding, 2009). The region is

79 characterized by a dipole mode, with southern flood and northern drought and *vice*

80 *versa* at decadal timescales. An additional sandwich pattern of arid central conditions,

81 bracketed by wetter conditions to the north and south, and *vice versa*, also likely

82 recurred over the instrumental observed period. An important question then is

83 whether such spatial pattern existed in the past, and at what time scales and how they

84 are manifested in geological records? The lack of well-dated high-resolution records

85 complicates the study of centennial- to decadal-scale climate dynamics and hinders

86 the understanding of spatial variation of monsoon precipitation and limits assessing

87 future climatic and environmental changes at these timescales.

88

89 The climate change has substantial impacts on the development of ancient cultures

90 (deMenocal, 2001, and references therein; Weiss, et al., 1993). Beyond all doubt, the

91 rise and fall of Neolithic cultures in China were closely linked with Holocene climate

92 change. Notably, the documented cultural remains reveal a continuum of cultural

93 periods prior to historical dynasties during the Holocene (from ~10.5 ka to ~3.5 ka) in

94 the central plains of China, without significant hiatuses between different cultural

95 periods (Li et al., 2013; Li et al., 2015a; Wang, 2014), a scenario quite different from

96 that in northern China (Li et al., 2007; Yang et al., 2015). Why are the cultural

97 remains so widely distributed in this central region and why are there no distinct

98 cultural shifts/hiatuses? Clarifying the relationship between the continued activity of

99 early civilizations and climate change might help adaptation and mitigation efforts to

100 ease societal vulnerability against climatic changes. A deeper understanding of these

101 climate-societal interrelationships requires a network of proximal well-dated records

102 of climatic and environmental dynamics from high-fidelity sites in the central plains

103 of China.

104

105 To help fill this gap, we present a precisely dated and highly resolved (temporal

106 resolution of 3-10 years) stalagmite isotope records from Magou Cave, Henan

107 Province, central China (figure 1). We reconstruct the Holocene history of the EASM,

108 characterize the climate instability during the Holocene Megathermal and investigate

109 possible physical mechanisms behind the climatic changes in the study region.

110 Finally, we examine possible links between civilization succession and climate

111 change.

2. Cave site and local climate

113 Magou Cave (113°23'E, 34°19'N, 422 m above sea level) is located 50 km southwest

114 of Zhengzhou City, Henan Province, China (figure 1). The cave formed in the

115 Ordovician limestone of the Ju-Ci-Shan Group. It was a closed cave without natural

116 entrance before it has been exposed and destroyed during quarrying activities in 2010.

117 The annual mean temperature is about 14.4℃, and the annual precipitation varies

118 between 421.3 and 1121.4 mm, with a mean of 721.2 mm from 1953-2010, as

119 observed at the nearest Xuchang meteorological station (113°52'E, 34°2'N, 47 km

120 southeast of the Cave site, http://www.geodata.cn). Precipitation falls mainly during

121 the summer monsoon season, with about 62% of the annual budget delivered between

122 June and September.

123

124 Straddling the boundary between the subtropical humid zone and the warm temperate

125 semi-humid zone in China, the EASM dictates the local climate and environment. In

126 summer, southerly winds from the low latitudes prevail and provide important

127 monsoonal precipitation; in winter, northerly winter monsoon winds bring cold, dry

128 air from mid- to high-latitudes regions (figure 1), defining a cold and relatively dry

129 winter climate regime. With these alternations of the summer and winter monsoons, a

130 distinctly warm-humid summer and cold-dry winter seasonality governs this region

131 (Cwa climate according to the Koeppen-Geiger classification, Peel et al. 2007).

132

133 The special geographical location of the cave leads to the heightened climate

134 sensitivity of this area, and the Central plain is the core region of agricultural

135 production and of great significance to China's food security (The Editorial

136 Committee of China Agricultural Statistical Yearbook, 2017). Regional climate

137 change has a significant impact on agricultural production (Wang et al., 2007).

138 Therefore, the study of climate dynamics in this region is of great significance not

139 only for understanding the spatial variability of Holocene climate across Eastern

140 China, but also for projecting and coping with future climate change.

141 **3. Stalagmites and methods**

142 Five stalagmites, MG-1, MG-2, MG-7, MG-40 and MG-64 have been retrieved from

143 Magou Cave and are for this study. After halving these stalagmites (figure 2 shows

144 the polished sections of the five stalagmites), about 50-60 mg powder subsamples

145 were drilled along the growth axis of each stalagmite and prepared for ^{230}Th-^{234}U-^{238}U

146 dating. The chemical separating procedure for uranium and thorium is similar to that

147 described in Edwards et al. (1987), and the details on instrumental measuring

148 protocols can be found in Cheng et al. (2013). A ^{230}Th/ ^{232}Th atomic ratio of

149 $4.4\pm2.2\times10^{-6}$ was used to correct for initial ^{230}Th. The measured data, the decay

150 constants and the calculated ages are listed in supplementary Table 1.

151

152 The micro-milling approach was used to extract sub-samples at different sampling

153 resolution. For stalagmite MG-1, the sampling intervals are 50 μm between 0 and 3.6

154 mm, 100 μm for the interval 3.6-7.6 mm, and 150 μm between 7.6 and 225.15 mm;

155 for stalagmite MG-2, the sampling intervals are 100 μm in the portion of 0-15 mm

156 and 200 μm between 15 and 139.6 mm. In stalagmites MG-40, MG-7 and MG-64 the

157 sampling intervals are 50 μm, 100 μm and 100 μm, respectively. A total of 3846

158 oxygen and carbon stable isotope analyses were performed using an IsoPrime 100

159 mass spectrometer equipped with a Multi-Prep Device at the Institute of Earth

160 Environment of the Chinese Academy of Sciences. All oxygen and carbon isotope

161 results are reported in delta (δ) notation. The standard results show that the precision

162 of $\delta^{18}O$ and $\delta^{13}C$ analyses are better than 0.15‰ and 0.12 ‰ (2σ), respectively.

163

164 The stable isotope data and most dates from stalagmites MG-1 and MG-40 have been

165 reported in an earlier study (Mao et al. 2016). Here we report two additional dates

166 from the base of MG-40, and five more dates from stalagmite MG-1 which improved

167 their chronologies significantly.

168 **4. Results**

169 **4.1 The U/Th chronology**

170 In total, sixty-six ^{230}Th dates were attained from the five stalagmites, with 23 dates

171 from MG-1, 11 dates from MG-2, 13 dates from MG-7, 8 dates from MG-40 and 11

172 dates from stalagmite MG-64. Given the high density of dates and relatively small

173 dating errors (most errors are <1%) and with most dates in stratigraphic order (figure

174 3), we use linear interpolation to establish depth-age chronologies for each stalagmite.

175 We also use the COPRA routine (Breitenbach et al., 2012) to test the reliability of the

176   linear chronology and find negligible differences between both approaches (figure 3).

177   The modeled chronologies indicate that MG-1 spans the time period from 4.88-10.36

178   ka, MG-2 from 5.84-7.77 ka, MG-40 from 6.91-11.48 ka and MG-64 from 1.11-5.43

179   ka. The ^{230}Th dates obtained from stalagmite MG-7 show three growth periods, i.e.,

180   from ~78.70 to 77.39 ka, 11.80 to 10.13 ka, and between ~8.20 and 7.74 ka. In this

181   study, we focus only on the Holocene section (11.80 to 10.13 ka) to attain the highest

182   resolved isotope profiles. The growth intervals of these stalagmites overlap for

183   different time windows (figure 3a).

184

185   The calculated growth rates of these stalagmites vary from 1.2 μm/year to 500

186   μm/year, with mean growth rates of 41.1 μm/year, 72.3 μm/year, 18.9 μm/year, 5.2

187   μm/year and 19.0 μm/year for stalagmites MG-1, MG-2, MG-7, MG-40 and MG-64,

188   respectively. The large variability observed in mean growth rates suggests that the

189   growth-controlling mechanisms (e.g. water pathway through the epikarst, drip rate,

190   degree of supersaturation of the dripwater, CO_2 degassing) differed for these

191   stalagmites. As shown in figure 3b, higher growth rates largely occurred during the

192   mid-Holocene (~8.0 - 4.8 ka BP), implying optimum conditions for speleothem

193   calcite deposition existed at the time.

194   **4.2 The δ^{18}O and δ^{13}C records**

195   Using the aforementioned micro-milling intervals, we achieved a mean temporal

196   resolution of 3.5 years, 2.5 years, 5.3 years, 9.2 years and 5.3 years for stalagmites

197   MG-1, MG-2, MG-7, MG-40 and MG-64, respectively, as calculated from their

198   chronologies. As shown in figure 4a, δ^{18}O varied from -7.8‰ to -12.8‰ in all

199   stalagmites. Generally, δ^{18}O decreased abruptly after 11.7 ka BP, and then gradually,

200   until 9.2 ka BP, without a clear long-term trend between 9.2 and 5.0 ka BP. Between

201   5.0 and 3.3 ka BP the δ^{18}O record consistently trended towards higher values. After

202   3.3 ka BP, the δ^{18}O values first decreased and then followed an increasing trend.

203   Superimposed on this long-term trend are prominent large-amplitude decadal-scale

204   oscillations. We build a composite δ^{18}O record (MG-composite, figure 5) by

205   combining the best dated and highest resolved sections of the individual δ^{18}O time

206   series of the five stalagmites of the overlapping periods. This composite δ^{18}O record

207   covers most of the Holocene, i.e., from 11.80 to 1.11 ka, with an average temporal

208   resolution of ~4 years.

209

210   The δ^{13}C records range from -7.0‰ to -11.5‰ and their variability largely follows

211   that of δ^{18}O, showing first a decreasing trend, then a stabilization during the mid-

212   Holocene, and finally increased and more variable values during the late Holocene

213   (figure 4b). The δ^{13}C values of stalagmite MG-40 are systematically ~1.0-1.2‰

214   heavier compared to those of stalagmites MG-1 and MG-7 during the overlap period

215   ~8.0 to ~11.5 ka BP, implying that the factors that influence the δ^{13}C signal differ

216   among the stalagmites.

217   **5. Discussion**

218   **5.1 Testing for isotope equilibrium deposition**

219   Given that the cave had no direct connection with the surface, both ventilation and

220   potential for evaporation in the cave were minimal, providing an exceptionally stable

221   microclimatic environment for the deposition of speleothem calcite under

222   (near-)isotope-equilibrium conditions. Within the quoted chronological confidence

223   limits, and considering the differences in temporal resolution, all δ^{18}O time series

224   show remarkable similarities during the overlapping interval between 11.7 and 5 ka

225 BP (figure 4a). The new time series also share similarities with a composite Holocene

226 $\delta^{18}O$ record from Laomudong/Dongshiya Caves (figure 5a, Zhang et al., 2018), both

227 situated ~180 km southwest of Magou Cave, and a Holocene $\delta^{18}O$ record from

228 Jiuxian Cave, located ~400 km west of Magou Cave (figure 5b, Cai et al., 2010). The

229 replication of all the $\delta^{18}O$ records suggests that these stalagmites were very likely

230 deposited under (near-)isotopic equilibrium conditions and influenced by similar

231 environmental processes (Dorale and Liu, 2009; Wang et al., 2001).

232

233 Our four stalagmites also show consistent variations in the $\delta^{13}C$ profiles in the

234 overlapping period (figure 4b), which supports the replication test discussed above,

235 although the $\delta^{13}C$ values of stalagmite MG-40 are systematically about 1.0-1.2 ‰

236 higher relative to those in stalagmites MG-1 and MG-7 over the interval prior ~8.1 ka

237 BP. This offset might result from differences in the proportion of seepage versus

238 fracture flow feeding the stalagmites. Higher $\delta^{13}C$ values in sample MG-40 might

239 indicate a larger influence of prior calcite precipitation in the epikarst in a faster-

240 emptying fracture-flow setting.

241

242 The different lines of evidence outlined above suggest that the samples from Magou

243 Cave were deposited with minimal kinetic influence and that their stable isotope

244 records primarily reflect regional scale climatic variability.

245

246 **5.2 The interpretation of speleothem calcite $\delta^{18}O$**

247 Stalagmite $\delta^{18}O$ is jointly controlled by $\delta^{18}O$ of dripwater (which reflects the sum of

248 all factors that control the water from its source to the stalagmite), and the

249 temperature inside the cave, provided that the stalagmite was formed under

250 (near-)isotopic equilibrium conditions (Hendy, 1971). Regarding the speleothem δ^{18}O

251 changes found in our stalagmites it is clear that temperature alone is insufficient to

252 explain the observed ca. five per mil amplitude. Experimental studies and theoretical

253 calculations (Coplen, 2007; Kim and O'Neil, 1997; O'Neil et al., 1969,) showed that

254 the temperature-dependent oxygen isotope fractionation between calcite and water is

255 about -0.23‰/°C. For northern China a lowering in annual mean temperature of about

256 2-3°C has been estimated from the warmest Holocene thermal maximum to the

257 coldest period of the Little Ice Age (Wang et al., 2001b). Thus, temperature changes

258 would explain at most ~0.7‰ of the observed δ^{18}O change in our records. Using the

259 cave-specific empirical water–calcite oxygen isotope fractionation relationship of -

260 0.177‰/°C of Tremaine et al. (2011) would reduce the explained change in

261 speleothem δ^{18}O further to only ~0.5‰. Thus, the observed changes in the Holocene

262 δ^{18}O time series from Magou Cave are mainly governed by the δ^{18}O signal of the

263 dripwater, i.e., by the history of the supplied moisture and related variations in the

264 amount-weighted δ^{18}O of meteoric precipitation above the cave.

265

266 It is worth to noting that we cannot strictly exclude any temperature effect on the

267 variation of speleothem calcite δ^{18}O because the variation of precipitation δ^{18}O might

268 be slightly altered by the temperature-dependent fractionation between dripwater and

269 speleothem calcite. Also, the Holocene temperature conundrum (Liu et al., 2014a),

270 i.e., the inconsistency between reconstructed cooling and inferred warming forced by

271 GHGs and ice sheet, limits our ability to constrain the temperature contribution to

272 variations in speleothem calcite δ^{18}O. We argue that changes in precipitation δ^{18}O

273 outweighed potential temperature effects, due to the small temperature-dependent

274 fractionation and low overall Holocene temperature changes (~2-3°C in

275   reconstructions, Wang et al., 2001, and ~1.5-2℃ in model simulations, Liu et al.,

276   2014a).

277

278   In monsoonal East Asia, multiple factors have been shown to affect the δ^{18}O of

279   dripwater (i.e. amount-weighted δ^{18}O of precipitation, changes in summer : winter

280   precipitation ratio (Wang et al., 2001), rainout between tropical oceanic sources and

281   the cave sites (Yuan et al., 2004), changes in the fraction of summer monsoon rainfall

282   with low δ^{18}O signal of the annual total (Cheng et al., 2009), and moisture source

283   changes (Cai et al., 2001, 2015; Tan, 2014)). The δ^{18}O signal in precipitation in the

284   EASM region reflects changes in the δ^{18}O of atmospheric vapor in the upstream

285   source regions over the Indian ocean (Baker et al. 2015; Liu et al., 2014b; Maher,

286   2008). Cai et al. (2017) further demonstrated that upstream convection, rather than

287   moisture source change, causes interannual variation in ASM precipitation δ^{18}O

288   values, corroborating the importance of the rainout effect on the isotopic composition

289   of precipitation. It should be noted that the mentioned rainout effect does not mean

290   that monsoonal precipitation δ^{18}O is negatively correlated with local rainfall amount

291   at all sites (i.e. the "amount effect", Dansgaard 1964), but rather Rayleigh

292   fractionation along the moisture transport pathway(s). Taken together, the rainout

293   history of moisture transported to the cave is essential for the interpretation of

294   speleothem calcite δ^{18}O. Lower δ^{18}O values generally indicate more distal moisture

295   source(s) in tandem with enhanced *en route* rainout linked to a stronger summer

296   monsoon and vice versa. Here, we largely follow the explanation by Cheng et al.

297   (2016) and use the terms 'strong monsoon' and 'weak monsoon' to refer to low and

298   high speleothem δ^{18}O values, respectively. We are cognizant of the argument that

299   changes in circulation and moisture sources (Cai et al., 2010, 2015; Hoffmann and

300   Heimann, 1997), and changes in recycling may contribute significantly to

301   precipitation $\delta^{18}O$ in our study region. We will discuss their influences in detail later.

5.3 Variability of speleothem $\delta^{18}O$ on different timescales

303   The MG-composite $\delta^{18}O$ profile spans the time period from 11.7 to 1.1 ka BP and

304   displays distinct variability on different timescales. At the beginning of the

305   reconstruction at ~11.7 ka BP, $\delta^{18}O$ values are relatively heavy (~-8.2 ‰). A shift

306   toward more depleted values occurred between 11.7 and ~11.5 ka BP, largely

307   corresponding with the end of the Younger Dryas event (Brauer et al., 2008).

308   Following this decrease, the $\delta^{18}O$ time series decreased gradually to -10.5 ‰, along

309   with large amplitude oscillations until ~9.25 ka BP. Thereafter, $\delta^{18}O$ fluctuated

310   around a mean value of -10.5 ‰ (stdev ±0.42, 1 σ) till ~5.0 ka BP, with a negligible

311   long-term trend of +0.03 ‰/1000 a. From ~5.0 ka BP to ~3.6 ka BP, the $\delta^{18}O$ record

312   quickly increased to ca. -9.8 ‰, with superimposed decadal to multi-decadal large

313   amplitude oscillations. Between ~3.4 ka BP and 2.7 ka BP, $\delta^{18}O$ values increased ca.

314   1.2 ‰ to the highest observed values of the entire time series, and then decreased

315   again until ca. 2.2 ka BP. After 2 ka BP and to the end of the record the $\delta^{18}O$ values

316   increased about 1 ‰.

317

318   To separate the modes of variability in the MG composite $\delta^{18}O$ time series we applied

319   Ensemble Empirical Mode Decomposition (EEMD) analysis method (Wu and Huang,

320   2009). Using this method, we obtain a total of 13 intrinsic functions (IFs, figure 6b-h).

321   The combined IFs 13-10 explain 20.3% of the variance and hint at variations of the

322    $\delta^{18}O$ reconstruction on sub-orbital timescales (figure 6b). IFs 9-8 (~26.1% of the

323   variance) show variability on timescales from sub-millennial to millennial years

324   (figure 6c). The combined IFs 7-6 (~22.7% of the total variance) display MG $\delta^{18}O$

325   variation at centennial timescales (figure 6d). IFs 5-4 vary on multi-decadal

326   timescales (figure 6f) and explain ~19.5% of the variance of the record. Finally, IFs 3-

327   1 show the decadal and shorter oscillations during periods with high growth rate

328   (figure 6h); these IFs include also some noise and must be treated with care.

329

330   We used a wavelet filter approach to further inspect the output of the EEMD analysis.

331   As shown in figure 6, the residual component, the 3000-500 year, 500-100 year, and

332   100-30 year band-pass outputs are highly correlated with the combined IFs 13-10, IFs

333   9-8, IFs 7-6, and IFs 5-4, with correlation coefficients of 0.96, 0.83, 0.90 and 0.92 (all

334   p values< 0.01) respectively, confirming that the combined intrinsic functions reflect

335   the variability of the MG composite $\delta^{18}O$ record on different timescales. Additionally,

336   the 1-30 years band-pass output is similar to the combined functions of IFs 1-3,

337   showing high-frequency oscillations of the MG-composite $\delta^{18}O$ record.

338

339   Comparison of the different IF variance with each other suggests comparable

340   variability of the precipitation $\delta^{18}O$ (under the assumption that speleothem $\delta^{18}O$

341   mainly reflects precipitation $\delta^{18}O$), on different timescales. Although IFs 1-3 could

342   explain ~11.4% of the record's variance, there is no discernible or distinct variation

343   during periods of low growth rate, highlighting the importance of record resolution on

344   the identification of sub-decadal variability. However, the IF 1-3 record reveals some

345   periods that reach annual to multi-annual resolution, even if age uncertainties hinder

346   us from discussing their variability in detail. The combined IFs 6-7 and IFs 8-9 (i.e.,

347   variations on 100-500- and 500-3000-years timescales) show slightly lower

348   amplitudes between ~8.5 and 4.9 ka BP, a period broadly aligned with the Holocene

349   Megathermal (Shi et al., 1992; Wang et al., 2001b). The EEMD analyses of the

350   published $\delta^{18}O$ records from nearby caves, i.e. LM/DSY and Jiuxian caves, show the

351   similar patterns in general (supplementary figure 1&2). This feature demonstrates

352   relatively stable climatic conditions at centennial to millennial timescales during this

353   warm time interval.

354

355   It is worth noting that higher $\delta^{18}O$ values centered at 1.4, 3.2, 4.3, 6.1, 8.1, 9.9, and

356   10.7 ka BP, indicative of weakened summer monsoon, align with the observed 500-

357   3000 years variability. These events agree with weak EASM events identified across

358   East Asia (Donges et al. 2015; Hong et al., 2003; Wang et al., 2005;), confirming

359   suggested links to dynamics in the North Atlantic (Bond et al., 2001, figure 6c). The

360   variability in the 100-500 years band (IFs 6-7, figure 6d) might be linked to shifts in

361   the mean position of the ITCZ in response to lower solar activity, but further work is

362   required to understand the underlying forcing (Gray et al. 2010 and references

363   therein). Meanwhile, the combined IFs 4-5 functions, comparable with the 30-100

364   years band-pass output, do not show such long-term pattern. Instead these IFs

365   highlight similar amplitude changes throughout the entire record, indicating continued

366   multi-decadal variability of the precipitation-driven $\delta^{18}O$ record. Exceptions with

367   lower amplitude are observed in periods with reduced deposition rates: ~11.7-10.7 ka

368   BP, ~10.1-8.6 ka BP, and ~2.8-1.1 ka BP. We tentatively propose that there are no

369   significant changes in the multi-decadal variability of the precipitation $\delta^{18}O$ signal,

370   implying relatively stable variability of Asian summer monsoon at multi-decadal

371   timescales which may be largely forced by the interaction of internal factors of

372   climate systems. While the IF results indicate continuous *relative* variability at these

373   timescales, high-resolution records with extreme age control are needed to test this

374   proposition.

375

5.4 Spatial variability of Holocene speleothem δ¹⁸O across East Asian monsoon

regions

The spatial feature of Holocene climate change in China, in particular, the Holocene

Optimum, has been first explored by An et al. (2000), subsequently by Ran and Feng

(2013), and recently by Zhou et al. (2016). However, no satisfactory mechanism has

been identified to interpret the observed phenomena in a holistic way.

Various Holocene speleothem δ¹⁸O records have been reported from south to north

China over the last 20 years (Cai et al., 2001; Hu et al., 2008; Wang et al., 2005; Yang

et al., 2019, reference therein; Zhang et al., 2018). These records are essential to

understand the spatial variability of Holocene environmental conditions across East

Asia. Recently, Yang et al. (2019) have tried to combine all Chinese Holocene

speleothem δ¹⁸O records into a single synthetic composite record, as well as to

compare synthetic records for southern and northern China. They find that all the

Holocene speleothem records share a common long-term trend, confirming the

dominant control of NHSI on EASM dynamics. However, significant disparity still

exists between southern and northern China. As shown in Fig. 4 in Yang et al. (2019),

the composite speleothem δ¹⁸O record from northern China (Fig. 4e) started to

increase much later (ca. 5.3 ka BP) than the composite record from southern China

(Fig. 4d) (it should be pointed out that the original figure in Yang et al. (2019) mixed

up the composite records of northern and southern China, personally confirmed with

Dr. YANG Xunlin, the corresponding author). Comparing the Holocene speleothem

δ¹⁸O record from Jiuxian Cave, central China, with other cave records from southern

China, Cai et al. (2010) found that the increasing trend in δ¹⁸O over the Holocene

400 commenced earlier in the southern monsoonal region, and later at higher latitudes.

401 Here, we compare the speleothem $\delta^{18}O$ records from three sites in central China, i.e.

402 Magou Cave, Dongshiya/Laomu caves, and Jiuxian Cave (figure 5). Within quoted

403 errors and considering the differences in resolution, these three records replicate their

404 millennial-scale to centennial variability. All three records indicate that speleothem

405 $\delta^{18}O$ was relatively lower during the early and middle Holocene (from ~9.0 to 5.0 ka

406 BP) and without a long-term trend, and only after ~5.0 ka BP speleothem $\delta^{18}O$ started

407 to increase, further corroborating the pattern proposed by Cai et al. (2010).

408

409 Why then do speleothem $\delta^{18}O$ records suggest an extended 'Holocene Moisture

410 Optimum' in northern China? We hypothesize that this can be explained by changes

411 in precipitation $\delta^{18}O$, which largely reflects the fraction of water vapor rained out

412 between tropical sources and the cave. The difference of the $\delta^{18}O$ in precipitation

413 between two sites from south to north can reflect the rainout between these two sites

414 (Hu et al., 2008), supposing there were no significant changes in moisture sources or

415 kinetic effects. Thus, the delayed increase of speleothem $\delta^{18}O$ in northern China

416 suggests that during the late mid-Holocene an increased fraction of water vapor rained

417 out between the southern (Heshang Cave) and central China sites (Magou Cave)

418 (supplementary figure 3). Some researchers argued that the increase of speleothem

419 $\delta^{18}O$ reflects a decreasing contribution of moisture from the Indian Ocean, or that

420 rainout upstream of the Indian monsoon region was reduced (Maher, 2008). This is

421 not at odds with our interpretation of increased precipitation in northern China during

422 the mid-Holocene, because we are concerned only about the precipitation $\delta^{18}O$

423 difference between (southern) upstream sites and Magou Cave. Taking all these lines

424 of evidence together, and consistent with reconstructions based on other archives

425   from central and northern China (Chen et al., 2015; Xiao et al., 2004; Wei et al.,

426   2020), it is likely that precipitation was higher from 8.5 ka BP to 5.3 ka BP, which

427   could be regarded as the Holocene Moisture Optimum in central China, and

428   diminished in the second half of the Holocene.

429

430   It is worth noting that two factors substantially influence the precipitation estimate.

431   One is the amount of moisture transported, because the precipitation amount is the

432   function of both available moisture and the fraction of water vapor that is rained out.

433   Another factor is the contribution of recycled water, because if sufficient recycled

434   water is available, the $\delta^{18}O$ signal of the water vapor *en route* might remain the same

435   (Rozanski et al., 1993). An increased contribution of recycled water would lead to

436   underestimation of precipitation amount. Increased temperature would lead to

437   increased atmospheric specific humidity and also increase evapotranspiration. It is

438   likely that from the early to mid-Holocene moisture transport and recycling were

439   increased, and that the precipitation $\delta^{18}O$ difference between sites alone may

440   underestimate the amount of precipitation during the middle Holocene. How and to

441   what degree these two factors affect the estimate of precipitation amount during the

442   Holocene warrants further study, including sophisticated model simulations. We

443   recognize that changes in moisture source might also affect the precipitation amount

444   estimate on a single trajectory. However, we refrain from further discussion, because

445   we qualitatively estimate the precipitation amount on a generally consistent trajectory

446   using the precipitation $\delta^{18}O$ difference between the upstream and cave sites across a

447   larger region. The likelihood of a changed moisture source seems relatively small

448   compared to other factors.

449

5.5 Variation of precipitation δ¹⁸O during the Holocene Megathermal and its

implications

During the Holocene, a period warmer than present, namely the Holocene

Megathermal (Fairbridge, 2009), has been identified around the northern Hemisphere,

albeit of variable timing and different amplitudes of temperature in different regions

(Johnsen et al., 2001; Kaufman et al., 2004; Shi et al., 1992; Wang, 2011). In China,

Shi et al. (1992) suggested that the Holocene Megathermal occurred between 8.5 and

3.0 ka BP, and the temperature increase may have been as high as 3℃ in northern

China and only 1℃ in southern China. It has also been suggested that this warm

period was not consistently warm and stable, but rather variable (Fang et al., 2011; Ge

et al., 2007; Peng et al., 2005; Wang et al., 2001b). Some discrepancies are apparent,

probably due to the different spatial domains and chronological control (He et al.,

2004).

Here we investigate the variability of speleothem δ¹⁸O during this Holocene warm

period in more detail. Between 8.5 and 4.9 ka BP the δ¹⁸O record from stalagmite

MG-1 shows a very weak and hardly discernable long-term trend (figure 7), similar to

the components identified with the EEMD and wavelet filtering analysis (IFs

$_{10+11+12+12+13}$ and residual in figure 6), indicating stable long-term climatic conditions

in central China. However, large-amplitude (1.0-1.5 per mil) high-frequency (intra-

decadal to multi-decadal) oscillations characterize this period. With the 15-year

weighted-average time series of the MG-1 δ¹⁸O record, fourteen weak monsoon

intervals (namely WMI 1 to WMI1 4) are identified with trough values exceeding 1.5

standard deviations of the mean of this interval (similar to the 8.2 event) (figure 7c).

475 The ages of the mid-points of these events are 8.29 ka BP, 8.12 ka BP, 7.71 ka BP,

476 7.67 ka BP, 7.35 ka BP, 7.08 ka BP, 6.57 ka BP, 6.25 ka BP, 6.08 ka BP, 6.00 ka BP,

477 5.79 ka BP, 5.50 ka BP, 5.35 ka BP, 5.18 ka BP. Within quoted dating uncertainty,

478 these events could align with the events identified from the δ^{18}O record from Dongge

479 Cave (figure 7b), and comparable fluctuations could be found in the δ^{18}O record from

480 Heshang Cave (figure 7a), although the amplitudes of these events are varied in

481 different records. The durations of these events varied from ~20 to ~70 years. The

482 weak monsoon interval 2, centered at 8.12 ka BP, lasted ca. 50 years, and is most

483 likely related to the 8.2 ka event (Cheng et al., 2009b; Liu et al., 2013). This WMI 2

484 shows a double-plunging structure if take the small trough at ~8.20 ka BP into

485 consideration. The 8.2 ka BP event is the most prominent Holocene excursion

486 observed in the Greenland ice cores (Alley et al., 1997). Its manifestation in Asian

487 monsoon precipitation δ^{18}O has been suggested to be brought about via a cold and

488 extended Siberian High, resulting in a southward shift of the mean position of the

489 ITCZ (Cheng et al., 2009b; Liu et al., 2013; Wang et al. 2004; Wang et al., 2005).

490

491 However, the amplitude of the 8.2 ka BP WMI 2 is the same or even smaller than

492 other weak monsoon intervals identified during the Holocene Megathermal,

493 suggesting that the variability of precipitation δ^{18}O in central China is affected by

494 other processes as well. A 200 year long, seasonally-resolved speleothem δ^{18}O record

495 from Dongshiya Cave (Zhao et al., 2018), suggests that, on annual to decadal

496 timescales, speleothem δ^{18}O (and by inference precipitation δ^{18}O) in central China is

497 related to the West Pacific Subtropical High (WPSH, Zhao et al., 2018), i.e., high

498 δ^{18}O values indicate a westward extension of the WPSH, and vice versa. If this

499 relation was still valid during the Holocene Megathermal, the identified WMIs may

500 be associated with substantial variations of the WPSH. Changes in the WPSH have

501 been linked to the SST in the tropical Indian Ocean and West Pacific (Sun and Ying,

502 1999; Wang et al., 2000; Wu et al., 2010; Xie et al., 2009). Others suggested that

503 changes in the WPSH might result via feedback processes from the EASM domain

504 (Hoskins, 1996; Liu et al., 2001). Recently, Fan et al. (2018) reported a high-

505 resolution SST time series from west Pacific warm pool. It indicates that there were

506 substantial variations of SST on centennial timescale (figure 7d), hinting the potential

507 linkage between the WMIs and temperature change in West Pacific, although we

508 cannot line up these oscillations in SST with WMIs in our record one by one due to

509 lower resolution and relatively larger age uncertainties of SST record.   Considering

510 that both, tropical SST and the EASM system play an important role in WPSH

511 dynamics, and that no significant excursions (except the 8.2 ka event) associated with

512 the WMIs are found in the northern high latitudes, we tentatively propose that these

513 WMI could be associated with surface temperature changes in the tropical Indian

514 Ocean and West Pacific, and that considerable SST changes occurred on centennial

515 timescale during the Holocene Megathermal.

516 **5.6 Variation of speleothem calcite δ^{13}C and its climate significance**

517 The δ^{13}C is a valuable proxy reflecting local environmental changes (Fohlmeister et

518 al., 2020; Lechleitner et al., 2017). Multiple factors (either individually or in

519 combination) may contribute to the speleothem δ^{13}C signal, including the isotopic

520 composition of soil CO_2, which reflects the vegetation activity and composition (i.e.,

521 C_3 vs C_4), the biomass, and microbial activity in the soil, dissolution of carbonate rock

522 (open system vs. closed system), and prior carbonate precipitate (PCP) in the epikarst

523 and/or the cave environment (Genty et al., 2006; Fohlmeister et al., 2020; Lechleitner

524 et al., 2017; McDermott, 2004; Ridley et al., 2015). As shown in figure 4, the long-

525   term $\delta^{13}C$ variations generally share similarities with $\delta^{18}O$, indicating both $\delta^{13}C$ and

526   $\delta^{18}O$ were affected by common forcings on different timescales, most likely reflecting

527   changes in local effective rainfall associated with the summer monsoon intensity.

528   Lower $\delta^{13}C$ values indicate intensified effective EASM rainfall and enhanced soil

529   CO_2 production and reduced PCP in the epikarst above the cave, whereas higher

530   values result from reduced microbial activity in the soil, and enhanced PCP under

531   drier conditions. While vegetation and soil dynamics likely play a role for the multi-

532   centennial to millennial scale trend in $\delta^{13}C$, the higher-frequency changes are

533   probably more directly related to PCP changes. The $\delta^{13}C$ profile also features

534   centennial-multi-decadal scale environmental changes that mirror those observed in

535   the $\delta^{18}O$ time series. This fact corroborates the notion that local moisture changes are

536   directly related to regional EASM dynamics (Liu et al., 2014b). There are also several

537   periods (e.g. 10.8-11.4 ka BP and 3.6-4.2 ka BP) showing anti-phase variation or

538   disparities in the $\delta^{13}C$ and $\delta^{18}O$ records. It's likely caused by the closed system

539   dissolution (Genty et al., 2001) resulted from the increased precipitation. However,

540   these inferences are only tentative and independent evidence (e.g. PCP-sensitive trace

541   element ratios) is required to verify this interpretation.

542   **5.7 Potential impact of climate change on cultural development in central China**

543   The relationship between climate and the fate of ancient cultures has long been the

544   research focus in academia. By aligning records of climate change and archeological

545   observations, many researches have linked the hiatus or 'collapse' of ancient cultures

546   to large and persistent climatic and environmental changes (Carolin et al. 2019; Chen

547   et al., 2005; Cullen et al. 2000; deMenocal, 2001; Haug et al., 2003; Hodell et al.,

548   1995; Kennett et al., 2012; Sinha et al., 2019; Weiss et al., 1993; Yang et al., 2015;

549   Zhang et al., 2008).

550

Located in the Central Plain with favorable climate and environment, Henan Province

is rich in Neolithic archaeological sites. Different to other regions in China, the

Neolithic cultures in this region (figure 8a) are consecutively developed without

cultural dislocation (Li et al., 2015a). However, these cultures still experienced

significant changes. While during the Lijiagou period only few Neolithic

archeological sites have been recorded in Henan Province, the number of sites

increased slightly during the Peiligang period, and subsequently significantly during

both the Yangshao and Longshan periods, while their number decreased strongly

during the Erlitou period (Li et al., 2013). Spatially, archaeological sites are

concentrated along the middle and lower reaches of rivers in western and central

Henan during the Peiligang and Erlitou periods, while during the Yangshao and

Longshan periods sites were dispersed more widely from the hilly to the lower plains.

The changes in the number of sites and their spatial distribution suggest that climatic

changes could have been an important factor influencing cultural development in

Henan province. Intensified EASM and increased precipitation, as indicated by our

stable isotope records (both $\delta^{18}O$ and $\delta^{13}C$), the growth frequency of the stalagmites

from Longfeng Cave (Wei et al., 2020) and the reconstructed precipitation using the

pollen records extracted from lake sediments (Chen et al., 2015, figure 8), and higher

temperatures during the early Holocene (10.5-7 ka BP, not shown here, Wang et al.,

2001) likely provided favorable environmental conditions for the development of the

Lijiagou to Peiligang cultures and supported the prosperous development of the

Yangshao and Longshan cultures. Reduced precipitation, possible in tandem with

lower temperatures, might have hastened the decline of the Erlitou culture, as

574 indicated by the reduced number of sites and distribution patterns in Henan Province

575 (Li et al., 2013).

576

577 Furthermore, changes in planted crop species and pollen assemblages suggest climate

578 change may have affected Neolithic cultural development in Henan Province. Plant

579 remains from Baligang site, Dengzhou in Henan Province, indicate that during the

580 Peiligang culture period the population cultivated rice and gathered fruits (Deng and

581 Gao, 2012). Subsistence strategies then changed to adopt a mixture of rice, foxtail

582 millet and common millet during the Yangshao and Longshan cultures with variable

583 proportions of these three crops, i.e., relatively increased millets during the early

584 Yangshao and late Longshan periods (Deng and Gao, 2012; Fu et al., 2010;). At the

585 same time, millets (adapted to drier climate compared to rice) are widely grown at the

586 northern sites. An increased proportion of millets likely suggests drier conditions

587 during the early Yangshao and the late Longshan periods, consistent with the

588 inference of precipitation changes from our stable isotope records and other proxy

589 records (figure 8), although we cannot exclude the potential influence of interplay

590 between northern foxtail millet-based cultures (i.e., Yangshao and Longshan) and

591 southern rice-growing cultures (i.e., Jujialing and Shijiahe) (Li et al., 2015b).

592

593 Taken together, it is most likely that the relatively moderate climatic shifts in Henan

594 Province, i.e., changes from subtropical humid to warm temperate semi-humid

595 climate, generally allowed consecutive development of ancient cultures in the Central

596 Plain, but modulated the livelihood and adaptation measures of these cultures.

597

6. Conclusions

As the transition zone between the subtropical humid and the warm temperate semi-humid climates, and today dominated by the summer monsoon, the central plain of China is a core area of modern agricultural production, as well as ancient civilization. At the same time, this region is sensitive to climate change. Based on the high-precision U-series-based chronologies from five stalagmites we developed highly resolved stable isotope time series covering the period from ~11.7 to 1.1 ka BP with an average resolution of ~4 years.

The new composite record reveals changes in precipitation $\delta^{18}O$ and demonstrates that summer monsoon intensity dominated the long-term dynamics of precipitation $\delta^{18}O$, which followed NHSI. EEMD and wavelet analysis show comparable variance of precipitation $\delta^{18}O$ on different timescales. Variance on timescales of 1-30 years is relatively low, reflecting the influence of the record's temporal resolution on these timescales. The reduced amplitudes of the 100-500 years and 500-3000 years components imply muted climate variability between 8.5-4.9 ka BP. Fourteen weak monsoon intervals were identified in this period, which largely corresponds to the Holocene Megathermal. Some of the identified weak monsoon intervals reveal positive $\delta^{18}O$ excursions larger than that associated with the 8.2 ka event. In the absence of cold excursions, as inferred for the 8.2 ka event, these EASM oscillations are tentatively linked to changes in tropical SST.

Aligning this record with archaeological observations, it seems likely that climatic changes influenced the development of ancient cultures. However, the moderate

622 regional climatic change during the discussed part of the Holocene allowed

623 continuous development of ancient cultures in Henan Province, central China.

624

625 **Acknowledgements**

References

632

633 Alley, R.B., Mayewski, P.A., Sowers, T., Stuiver, M., Taylor, K.C., Clark, P.U.,

634 1997. Holocene climatic instability: Aprominent, widespread event 8200 yr ago.

635 Geology 25(6), 483-486.

636 An, Z., Porter, S.C., Kutzbach, J.E., Wu, X., Wang, S., Liu, X., Li, X., Zhou W.,

637 2000. Asynchronous Holocene optimum of the East Asian monsoon. Quaternary

638 Science Reviews 19, 743-762.

639 An, Z., Colman, S.M., Zhou, W., Li, X., Brown, E.T., Jull, A.J.T., Cai, Y., Huang, Y.,

640 Lu, X., Chang, H., Song, Y., Sun, Y., Xu, H., Liu, W., Jin, Z., Liu, X., Cheng, P., Liu,

641 Y., Ai, L., Li, X., Liu, X., Yan, L., Shi, Z., Wang, X., Wu, F., Qiang, X., Dong, J., Lu,

642 F., Xu, X., 2012. Interplay between the Westerlies and Asian monsoon recorded in

643 Lake Qinghai sediments since 32 ka. Scientific Reports 2,619

644 Bond, G., Kromer, B., Beer, J., Muscheler, R., Evans, M.N., Showers, W., Hoffmann,

645 S., Lotti-Bond, R., Hajdas, I., Bonani, G., 2001. Persistent Solar Influence on North

646 Atlantic Climate During the Holocene. Science 294, 2130-2136.

647 Breitenbach, S.F.M., Rehfeld, K., Goswami, B., Baldini, J.U.L., 2012. Constructing

648 proxy records from age models (COPRA). Climate of the Past 8, 1765e1779.

649 Cai, Y., Zhang, M., Peng, Z., Lin, Y., An, Z., Zhang, Z., Cao, Y., 2001. The δ^{18}O

650 variation of a stalagmite from Qixing Cave, Guizhou Province and indicated climate

651 change during the Holocene. Chinese Science Bulletin 46(22), 1904-1908.

652 Cai, Y., Tan, L., Cheng, H., An, Z., Edwards, R.L., Kelly, M.J., Kong, X., Wang, X.,

653 2010. The variation of summer monsoon precipitation in central China since the last

654 deglaciation. Earth and Planetary Science Letters 291, 21-31.

655 Cai, Y., Fung, I.Y., Edwards, R.L., An, Z., Cheng, H., Lee, J.-E., Tan, L., Shen, C.-C.,

656 Wang, X., Day, J.A., 2015. Variability of stalagmite-inferred Indian monsoon

657 precipitation over the past 252,000 y. Proceedings of the National Academy of

658 Sciences 112, 2954-2959.

659 Cai, Z., Tian, L., Bowen, G.J., 2017. ENSO variability reflected in precipitation

660 oxygen isotopes across the Asian Summer Monsoon region. Earth and Planetary

661 Science Letters 475, 25-33.

662 Carolin, S.A., Walker, R.T., Day, C.C., Ersek, V., Sloan, R.A., Dee, M.W., Talebian,

663 M., Henderson, G.M., 2019. Precise timing of abrupt increase in dust activity in the

664 Middle East coincident with 4.2 ka social change. Proceedings of the National

665 Academy of Sciences 116, 67-72.

666 Chen, F., Xu, Q., Chen, J., Birks, H.J.B., Liu, J., Zhang, S., Jin, L., An, C., Telford,

667 R.J., Cao, X., Wang, Z., Zahng, X., Selvaraj, K., Lü, H., Li, Y., Zheng, Z., Wang, H.,

668 Zhou, A., Dong, G., Zhang, J., Huang, X., Bloemendal, J., Rao, Z., 2015. East Asian

669 summer monsoon precipitation variability since the last deglaciation. Scientific

670 Reports http://dx.doi.org/10.1038/srep11186.

671 Chen, Z., Wang, Z., Schneiderman, J., Taol, J., Cail, Y., 2005. Holocene climate

672 fluctuations in the Yangtze delta of eastern China and the Neolithic response. The

673 Holocene 15, 915-924.

674 Cheng, H., Edwards, R.L., Broecker, W.S., Denton, G.H., Kong, X., Wang, Y.,

675 Zhang, R., Wang, X., 2009a. Ice Age Terminations. Science 326, 248-252.

676 Cheng, H., Fleitmann, D., Edwards, R.L., Wang, X., Cruz, F.W., Auler, A.S.,

677 Mangini, A., Wang, Y., Kong, X., Burns, S.J., Matter, A., 2009b. Timing and

678   structure of the 8.2 kyr B.P. event inferred from $\delta^{18}O$ records of stalagmites from

679   China, Oman, and Brazil. Geology 37, 1007-1010.

680   Cheng, H., Lawrence Edwards, R., Shen, C.-C., Polyak, V.J., Asmerom, Y.,

681   Woodhead, J., Hellstrom, J., Wang, Y., Kong, X., Spötl, C., Wang, X., Calvin

682   Alexander Jr, E., 2013. Improvements in ^{230}Th dating, ^{230}Th and ^{234}U half-life values,

683   and U–Th isotopic measurements by multi-collector inductively coupled plasma mass

684   spectrometry. Earth and Planetary Science Letters 371–372, 82-91.

685   Cheng, H., Edwards, R.L., Sinha, A., Spötl, C., Yi, L., Chen, S., Kelly, M., Kathayat,

686   G., Wang, X., Li, X., 2016. The Asian monsoon over the past 640,000 years and ice

687   age terminations. Nature 534, 640-646.

688   Coplen T., 2007. Calibration of the calcite–water oxygen-isotope geothermometer at

689   Devils Hole, Nevada, a natural laboratory. Geochimica et Cosmochimica Acta 71,

690   3948–3957.

691   Cullen, H.M., deMenocal, P.B., Hemming, S., Hemming, G., Brown, F.H.,

692   Guilderson, T., Sirocko, F., 2000. Climate change and the collapse of the Akkadian

693   empire: Evidence from the deep sea. Geology 28, 379-382.

694   Deevey, E.S., and Flint, R.F., 1957. Postglacial Hypsithermal interval. Science, 125,

695   182–185.

696   deMenocal, P.B., 2001. Cultural Responses to Climate Change During the Late

697   Holocene. Science 292, 667-673.

698   Den, Z.H. and Gao, Y., 2012, The analysis of archaeobotanical remains from

699   Baligang site, Dengzhou, Henan Province. Cultural Relics in Southern China, 1:162-

700   169. In Chinese with English Abstract.

701 Ding, Y., Sun, Y., Wang, Z., Zhu, Y., Song, Y., 2009. Inter- decadal variation of the

702 summer precipitation in China and its association with decreasing Asian summer

703 monsoon Part II: Possible causes. International Journal of Climatology 29, 1926-

704 1944.

705 Donges, J.F., Donner, R., Marwan, N., Breitenbach, S.F., Rehfeld, K., Kurths, J.,

706 2015. Non-linear regime shifts in Holocene Asian monsoon variability: potential

707 impacts on cultural change and migratory patterns. Climate of the Past 11, 709-741.

708 Dorale, J.A., Liu, Z., 2009. Limitations of Hendy test criteria in judging the

709 paleoclimatic suitability of speleothems and the need for replication. Journal of Cave

710 and Karst Studies 71, 73-80.

711 Dreybrodt, W., 2008. Evolution of the isotopic composition of carbon and oxygen in a

712 calcite precipitating H_2O-CO_2-$CaCO_3$ solution and the related isotopic composition of

713 calcite in stalagmites. Geochimica et Cosmochimica Acta 72, 6198-6198.

714 Dykoski, C.A., Edwards, R.L., Cheng, H., Yuan, D., Cai, Y., Zhang, M., Lin, Y.,

715 Qing, J., An, Z., Revenaugh, J., 2005. A high-resolution, absolute-dated Holocene and

716 deglacial Asian monsoon record from Dongge Cave, China. Earth and Planetary

717 Science Letters 233, 71-86.

718 Edwards, R.L., Chen, J., Wasserburg, G.J., 1987. ^{238}U-^{234}U-^{230}Th-^{232}Th systematic

719 and the precise measurement of time over the past 500,000 years. Earth and Planetary

720 Science Letters 81, 175-192.

721 Fairbridge, R.W., 2009. Hypsithermal, in: Gornitz, V. (Ed.), Encyclopedia of

722 Paleoclimatology and Ancient Environments. Springer Netherlands, Dordrecht, pp.

723 451-452.

724   Fan, W., Jian, Z., Chu, Z., Dang, H., Wang, Y., Bassinot, F., Han, X., Bian, Y., 2018.

725   Variability of the Indonesian Throughflow in the Makassar Strait over the Last 30 ka.

726   Scientific Reports 8, 5678.

727   Fang, X., Hou, G., 2011. Synthetically reconstructed Holocene temperature change in

728   China. Scientia Geographica Sinica 31, 385-393. In Chinese with English abstract.

729   Fohlmeister, J., Riavo G. Voarintsoa, N., Lechleitner, F.A., Boyd, M., Brandtstätter,

730   S., Jacobson, M.J., Oster, J., 2020. Main Controls on the Stable Carbon Isotope

731   Composition of Speleothems, Geochimica et Cosmochimica Acta, doi:

732   https://doi.org/10.1016/j.gca.2020.03.042.

733   Fu, X., Jin, S., Hu, Y., Ma, Z., Pan, J., Wang, C., Agricultural development and

734   palaeodietary study of Gouwan site, Xichuan, Henan. Chinese Science Bulletin, 2010,

735   55: 614-620, doi: 10.1007/s11434-009-06215

736   Ge, Q., Wang, S., Wen, X., Shen, C., Hao, Z., 2007. Temperature and precipitation

737   changes in China during the Holocene. Advances in Atmospheric Sciences 24, 1024-

738   1036.

739   Genty, D., Blamart, D., Ghaleb, B., Plagnes, V., Causse, C., Bakalowicz, M., Zouari,

740   K., Chkir, N., Hellstrom, J., Wainer, K., Bourges, F., 2006. Timing and dynamics of

741   the last deglaciation from European and North African delta C-13 stalagmite profiles -

742   comparison with Chinese and South Hemisphere stalagmites. Quaternary Science

743   Reviews 25, 2118-2142.

744   Haug, G.H., Gu¨nther, D., Peterson, L.C., Sigman, D.M., Hughen, K.A.,

745   Aeschlimann, B., 2003. Climate and the Collapse of Maya Civilization. Science 299,

746   1731-1735.

747 He, Y., Theakstone, W. H., Zhang, Z., Zhang, D., Yao, T., Chen, T., Shen, Y., Pang,

748 H. 2004, Asynchronous Holocene climatic change across China. Quaternary

749 Research, 61, 52–63.

750 Hendy, C.H., 1971. The isotopic geochemistry of speleothems--I. The calculation of

751 the effects of different modes of formation on the isotopic composition of

752 speleothems and their applicability as palaeoclimatic indicators. Geochimica et

753 Cosmochimica Acta 35, 801-824.

754 Hodell, D.A., Curtis, J.H., Brenner, M., 1995. Possible role of climate in the collapse

755 of Classic Maya civilization. Nature 375, 391-394.

756 Hoffmann, G., Werner, M., Heimann, M., 1998. Water isotope module of the

757 ECHAM atmospheric general circulation model: A study on timescales from days to

758 several years. Journal of Geophysical Research, 103 (No. D14): 16871-16896.

759 Hong, Y., Hong, B., Lin, Q., Zhu, Y., Shibata, Y., Hirota, M., Uchida, M., Leng, X.,

760 Jiang, H., Xu, H., 2003. Correlation between Indian Ocean summer monsoon and

761 North Atlantic climate during the Holocene. Earth and Planetary Science Letters 211,

762 371-380.

763 Hoskins, B.J., 1996. On the existence and strength of the summer subtropical

764 anticyclones. Bulletin of the American Meteorological Society 77:1287–1292.

765 Hou, J., Li, C.-G., Lee, S., 2019. The temperature record of the Holocene: progress

766 and controversies. Science Bulletin 64, 565-566.

767 Hu, C., Henderson, G.M., Huang, J., Xie, S., Sun, Y., Johnson, K.R., 2008.

768 Quantification of Holocene Asian monsoon rainfall from spatially separated cave

769 records. Earth and Planetary Science Letters 266, 221-232.

770 Johnsen, S., Dahl-Jensen, D., Gundestrup, N., Steffensen, J., Clausen, H., Miller, H.,

771 Masson-Delmotte, V., Sveinbjornsdottir, A., White, J., 2001. Oxygen isotope and

772 palaeotemperature records from six Greenland ice-core stations: Camp Century, Dye-

773 3, Grip, GISP2, Renland and Northgrip. Journal of Quaternary Science 16, 299–307.

774 Kaufman, D.S., Ager, T.A., Anderson, N.J., Anderson, P.M., Andrews, J.T., Bartlein,

775 P.J., Brubaker, L.B., Coats, L.L., Cwynar, L.C., Duvall, M.L., Dyke, A.S., Edwards,

776 M.E., Eisner, W.R., Gajewski, K., Geirsdóttir, A., Hu, F.S., Jennings, A.E., Kaplan,

777 M.R., Kerwin, M.W., Lozhkin, A.V., MacDonald, G.M., Miller, G.H., Mock, C.J.,

778 Oswald, W.W., Otto-Bliesner, B.L., Porinchu, D.F., Rühland, K., Smol, J.P., Steig,

779 E.J., Wolfe, B.B., 2004. Holocene thermal maximum in the western Arctic (0–

780 180°W). Quaternary Science Reviews 23, 529-560.

781 Kennett, D.J., Breitenbach, S.F.M., Aquino, V.V., Asmerom, Y., Awe, J., Baldini,

782 J.U.L., Bartlein, P., Culleton, B.J., Ebert, C., Jazwa, C., Macri, M.J., Marwan, N.,

783 Polyak, V., Prufer, K.M., Ridley, H.E., Sodemann, H., Winterhalder, B., Haug, G.H.,

784 2012. Development and Disintegration of Maya Political Systems in Response to

785 Climate Change. Science 338, 788-791.

786 Kim, S.-T., O'Neil, J.R., 1997. Equilibrium and nonequilibrium oxygen isotope

787 effects in synthetic carbonates. Geochimica et Cosmochimica Acta 61, 3461-3475.

788 Lechleitner F.A., Breitenbach S.F.M., Cheng H., Plessen B., Rehfeld K., Goswami B.,

789 Marwan N., Eroglu D., Adkins J.F., Haug G.H., 2017. Climatic and in-cave

790 influences on $\delta^{18}O$ and $\delta^{13}C$ in a stalagmite from northeastern India through the last

791 deglaciation. Quaternary Research 88, 458-471, doi: 10.1017/qua.2017.72

792 Li, B., Wen, X., Qiu, S., 2007, Phases of Environmental Evolution Indicated by

793 Primary Chemical Elements and Paleontological Records in the Upper Pleistocene-

794   Holocene Series for the Salawusu River Valley, China. Acta Geologica Sinica

795   81(4):555–565

796   Li, K., Ma, C., Gao, W., Li, S., Li, Z., Pan, Y., 2015a, Progress and trend of Holocene

797   environmental archaeology in Henan Province. Progress in Geography, 34 (7): 883-

798   897, doi: 10.18306/dlkxjz.2015.07.010

799   Li, X., Shen, H., Tian, J., 2007, The Influences of Environment Evolution on Ancient

800   Culture Development in the Northern Part of China. Journal of Hebei Normal

801   University/Natural Science Edition, 31(5): 680-685. In Chinese with English abstract.

802   Liu, Y., Henderson, G., Hu, C., Mason, A., Charnley, N., Johnson, K., Xie, S., 2013.

803   Links between the East Asian monsoon and North Atlantic climate during the 8,200

804   year vent. Nature Geoscience 6, 117-120.

805   Liu, Y., Wu, G., Liu, H., Liu, P., 2001. Condensation heating of the Asian summer

806   monsoon and the subtropical anticyclone in the Eastern Hemisphere. Climate

807   Dynamics 17(4):327–338

808   Li, Z., Zhu, C., Wu, G., Zheng, C., Shao, S., Feng, F., Wang, Y., 2013. Spatial and

809   temporal distribution of prehistoric human sites and its driving factors in Henan

810   Province. Acta Geographica Sincia, 68(11): 1527-1537. In Chinese with English

811   Abstract.

812   Li, Z., Zhu, C., Yuan, S., Xu, J., Wu, G., Wang, H., Guo, Z., 2015b, Geographical

813   distribution, diffusion and subsistence variation of prehistoric cultures in Nanyang

814   Basin, Henan Province. Acta Geographica Sinica, 70(1):143-156. In Chinese with

815   English Abstract.

816   Liu, Z., Zhu, J., Rosenthal, Y., Zhang, X., Otto-Bliesner, B.L., Timmermann, A.,

817   Smith, R.S., Lohmann, G., Zheng, W., Timm, O.E., 2014a. The Holocene temperature

818   conundrum. Proceedings of the National Academy of Sciences 111, E3501-E3505.

819   Liu, Z., Wen, X., Brady, E., Otto-Bliesner, B., Yu, G., Lu, H., Cheng, H., Wang, Y.,

820   Zheng, W., Ding, Y., 2014b. Chinese cave records and the East Asia summer

821   monsoon. Quaternary Science Reviews 83, 115-128.

822   Maher, B.A., 2008. Holocene variability of the East Asian summer monsoon from

823   Chinese cave records: a re-assessment. The Holocene 18, 861-866.

824   Mao, R., Cai, Y., Ma, L., Cheng, X., 2016. Early to mid-Holocene paleoclimatic

825   changes recorded by the stalagmites from the Magou Cave, Henan Province. Journal

826   of Earth Environment, 7(3): 254-268. In Chinese with English abstract.

827   McDermott, F., 2004. Palaeo-climate reconstruction from stable isotope variations in

828   speleothems: a review. Quaternary Science Reviews 23, 901–918.

829   O'Neil, J.R., Clayton, R.N., Mayeda, T.K., 1969. Oxygen isotope fractionation in

830   divalent metal carbonates. The Journal of Chemical Physics 51(12), 5547-5558.

831   Peng, X., Zhong, W., Zhao, Y., Xue, J., 2005. Preliminary research in the Holocene

832   Hypsithermal climate change. Journal of South China Normal University: Natural

833   Science Edition, (2): 52–60.

834   Ran, M., Feng, Z., 2013. Holocene moisture variations across China and driving

835   mechanisms: A synthesis of climatic records. Quaternary International 313, 179-193.

836   Ridley, H.E., Asmerom, Y., Baldini, J.U.L., Breitenbach, S.F.M., Aquino, V.V.,

837   Prufer, K.M., Culleton, B.J., Polyak, V., Lechleitner, F.A., Kennett, D.J., Zhang,

838   M.H., Marwan, N., Macpherson, C.G., Baldini, L.M., Xiao, T.Y., Peterkin, J.L., Awe,

839   J., Haug, G.H., 2015. Aerosol forcing of the position of the intertropical convergence

840   zone since AD 1550. Nature Geoscience 8, 195-200.

841   Rozanski, K., Araguas-Araguas, L., Gonfiantini, R., 1993. Isotopic patterns in modern

842   global precipitation. Geophysical Monography 78, 1-36.

843   Shi, Y., Kong, Z., Wang, S., Tang, L., Wang, F., Yao, T., Zhao, X., Zhang, P., Shi, S.,

844   1992. Basic features of climates and environments during Holocene Megathermal in

845   China. In: Shi, Y.F., Kong, Z.C. (Eds.), The Climates and Environments of Holocene

846   Megathermal in China. China Ocean Press, Beijing, pp. l–18. in Chinese.

847   Sinha, A., Kathayat, G., Weiss, H., Li, H., Cheng, H., Reuter, J., Schneider, A.W.,

848   Berkelhammer, M., Adalı, S.F., Stott, L.D., 2019. Role of climate in the rise and fall

849   of the Neo-Assyrian Empire. Science advances 5, eaax6656.

850   Sun, S., Ying, M., 1999. Subtropical high anomalies over the western Pacific and its

851   relations to the Asian monsoon and SST anomaly. Advances in Atmospheric Sciences

852   16, 559-568.

853   Tan, M., 2014. Circulation effect: response of precipitation $\delta^{18}O$ to the ENSO cycle in

854   monsoon regions of China. Climate Dynamics 42, 1067-1077.

855   The Editorial Committee of China Agricultural Statistical Yearbook. 2017, China

856   Agriculture Yearbook. China Agriculture Press, Beijing.

857   Tremaine, D.M., Froelich, P.N., Yang, W., 2011. Speleothem calcite farmed in situ:

858   Modern calibration of $\delta^{18}O$ and $\delta^{13}C$ paleoclimate proxies in a continuously-

859   monitored natural cave system. Geochimica et Cosmochimica Acta 75, 4929-4950.

860   Wang, B., Wu, R., Fu, X., 2000. Pacific–East Asian teleconnection: how does ENSO

861   affect East Asian climate? Journal of Climate 13, 1517-1536.

862 Wang, J., Zhu, Y., Liu, H., 2007, Main agrometeorological disasters and their impact

863 in recent 28 years in Henan. Meteorological and Environmental Sciences 30, 9-11.

864 Wang, S., Gong, D., Zhu, J., 2001b. Twentieth-century climatic warming in China in

865 the context of the Holocene. The Holocene 11, 313-321.

866 Wang, S., 2011. Holocene Megathermal. Advances in Climate Change Research 7(5):

867 383-384.

868 Wang, X., Auler, A.S., Edwards, R.L., Cheng, H., Cristalli, P.S., Smart, P.L.,

869 Richards, D.A., Shen, C.-C., 2004. Wet periods in northeastern Brazil over the past

870 210 kyr linked to distant climate anomalies. Nature 432, 740-743.

871 Wang, Y., Cheng, H., Edwards, R.L., An, Z., Wu, J., Shen, C.-C., Dorale, J.A., 2001a.

872 A high-resolution absolute-dated late Pleistocene Monsoon record from Hulu cave,

873 China. Science 294, 2345-2348.

874 Wang, Y., Cheng, H., Edwards, R.L., He, Y., Kong, X., An, Z., Wu, J., Kelly, M.J.,

875 Dykoski, C.A., Li, X., 2005. The Holocene Asian Monsoon: Links to Solar Changes

876 and North Atlantic Climate. Science 308, 854-857.

877 Wang Y., 2014. On the research progress of Lijiagou site in Xinmi City and other

878 related problems. Cultural Relics of Central China, (1): 20-24.

879 Wei, Y., Cai, Y., Cheng, X., Xue, G., Lu, Y., Ma, L., Huang, S., He, M., Cheng, H.,

880 Edwards, R.L., 2020. Holocene and deglaciation hydroclimate changes in northern

881 China as inferred from stalagmite growth frequency. Global and Planetary Change

882 195, 103360.

883 Weiss, H., Courty, M.A., Wetterstrom, W., Guichard, F., Senior, L., Meadow, R.,

884 Curnow, A., 1993. The Genesis and Collapse of Third Millennium North

885 Mesopotamian Civilization. Science 261, 995-1004.

886   Wu, B., Li, T., Zhou, T., 2010, Relative contributions of the Indian ocean and local

887   SST anomalies to the maintenance of the western north Pacific anomalous anticyclone

888   during the El Niño decaying summer. Journal of Climate 23(11):2974–2986

889   Wu, Z., Huang, N., 2009, Ensemble Empirical Mode Decomposition: A noise-assisted

890   data analysis method. Advances in Data Analysis and Classification 1:1–41.

891   Xie, S., Hafner, J., Tokinaga, H., Du, Y., Huang, G., Sampe, T., 2009, Indian ocean

892   capacitor effect on Indo-Western Pacific climate during the summer following El

893   Niño. Journal of Climate 22(3):730–747

894   Xiao, J., Xu, Q., Nakamura, T., Yang, X., Liang, W., Inouchi, Y., 2004. Holocene

895   vegetation variation in the Daihai Lake region of north-central China: a direct

896   indication of the Asian monsoon climatic history. Quaternary Science Reviews 23,

897   1669-1679.

898   Yang, X., Scuderi, L.A., Wang, X., Scuderi, L.J., Zhang, D., Li, H., Forman, S., Xu,

899   Q.H., Wang, R., Huang, W., Yang, S., 2015. Groundwater sapping as the cause of

900   irreversible desertification of Hunshandake Sandy Lands, Inner Mongolia, northern

901   China. Proceedings of the National Academy of Sciences 112, 702-706.

902   Yang, X., Yang, H., Wang, B., Huang, L.-J., Shen, C.-C., Edwards, R.L., Cheng, H.,

903   2019. Early-Holocene monsoon instability and climatic optimum recorded by Chinese

904   stalagmites. The Holocene 29, 1059-1067.

905   Yuan, D., Cheng, H., Edwards, R.L., Dykoski, C.A., Kelly, M.J., Zhang, M., Qing, J.,

906   Lin, Y., Wang, Y., Wu, J., Dorale, J.A., An, Z., Cai, Y., 2004. Timing, Duration, and

907   Transitions of the Last Interglacial Asian Monsoon. Science 304, 575-578.

908   Zhang, D., 2003. Climatic Differences in China during the Holocene Indicated by the

909   Various Climatic Proxy Data from Different Parts of China. Journal of Glaciology

910   and Geocryology, 25(1): 11-18.

911   Zhang, N., Yang, Y., Cheng, H., Zhao, J., Yang, X., Liang, S., Nie, X., Zhang, Y.,

912   Edwards, R.L., 2018. Timing and duration of the East Asian summer monsoon

913   maximum during the Holocene based on stalagmite data from North China. The

914   Holocene 28, 1631-1641.

915   Zhang, P., Cheng, H., Edwards, R.L., Chen, F., Wang, Y., Yang, X., Liu, J., Tan, M.,

916   Wang, X., Liu, J., An, C., Dai, Z., Zhou, J., Zhang, D., Jia, J., Jin, L., Johnson, K.R.,

917   2008. A Test of Climate, Sun, and Culture Relationships from an 1810-Year Chinese

918   Cave Record. Science 322, 940-942.

919   Zhao, J., Cheng, H., Yang, Y., Tan, L., Spötl, C., Ning, Y., Zhang, H., Cheng, X.,

920   Sun, Z., Li, X., Li, H., Liu, W., Edwards, R.L., 2019. Reconstructing the western

921   boundary variability of the Western Pacific Subtropical High over the past 200 years

922   via Chinese cave oxygen isotope records. Climate Dynamics 52, 3741-3757.

923   Zhou, X., Sun, L., Zhan, T., Huang, W., Zhou, X., Hao, Q., Wang, Y., He, X., Zhao,

924   C., Zhang, J., 2016. Time-transgressive onset of the Holocene Optimum in the East

925   Asian monsoon region. Earth and Planetary Science Letters 456, 39-46.

926

927   Figure 1.
928
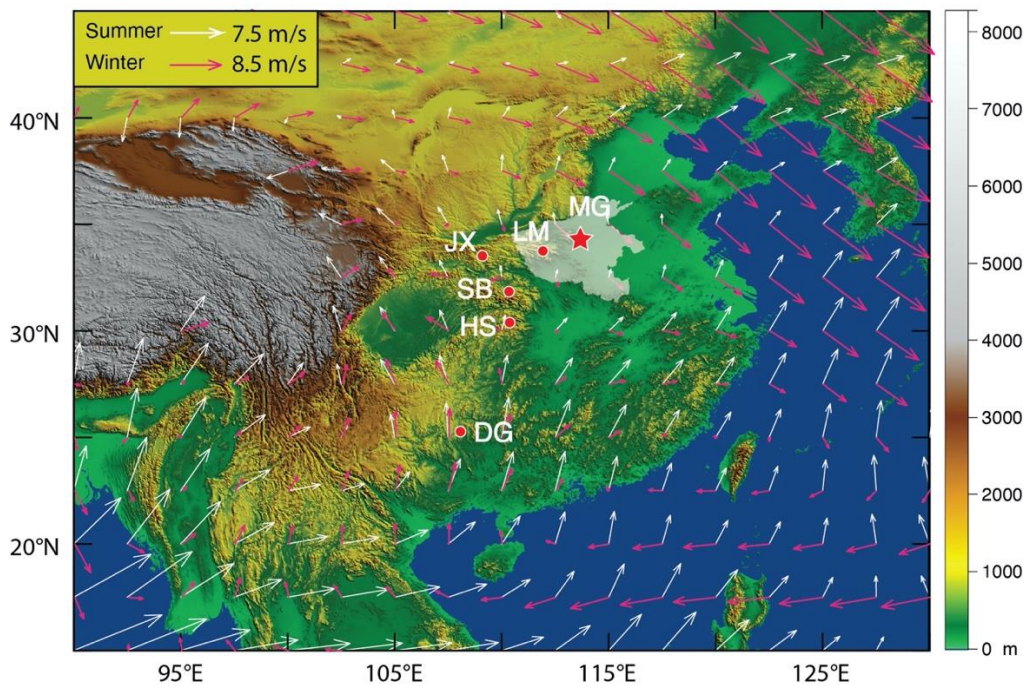
929
930   **Figure 1**: Overview map with the location of the studied cave and relevant records.

931   The topographic map is based on GTOPO 30 data (U.S. Geological Survey's EROS

932   (Earth Resources Observation and Science;

933   http://eros.usgs.gov/#/Find_Data/Products_and_Data _Available/gtopo30_info) Data

934   Center). White and purple arrows indicate mean summer and winter wind fields at

935   850 hPa from 1981 to 2010 (NCEP Reanalysis Derived data provided by

936   NOAA/OAR/ESRL PSD, Boulder, Colorado, USA, http://www.esrl.noaa.gov/psd/,

937   Kistler et al., 2001). The location of Magou Cave (MG) is denoted by the red star

938   (113°23'E, 34°19'N, ~422 m a.s.l.), all other records are denoted by red circles: LM:

939   Laomu Cave/Dongshiya Cave, 111°31'E, 33°48'N, ~840 m a.s.l.; JX: Jiuxian Cave,

940   109°6'E, 33°34'N, ~1495 m a.s.l.; SB: Sanbao Cave, 110°26'E, 31°40'N, ~1900 m

941   a.s.l.; HS: Heshang Cave, 110°25'E, 30°27'N, ~294 m a.s.l.; DG: Dongge Cave,

942   108°5'E, 25°17'N, ~680 m a.s.l. The white shaded area indicates the Henan Province,

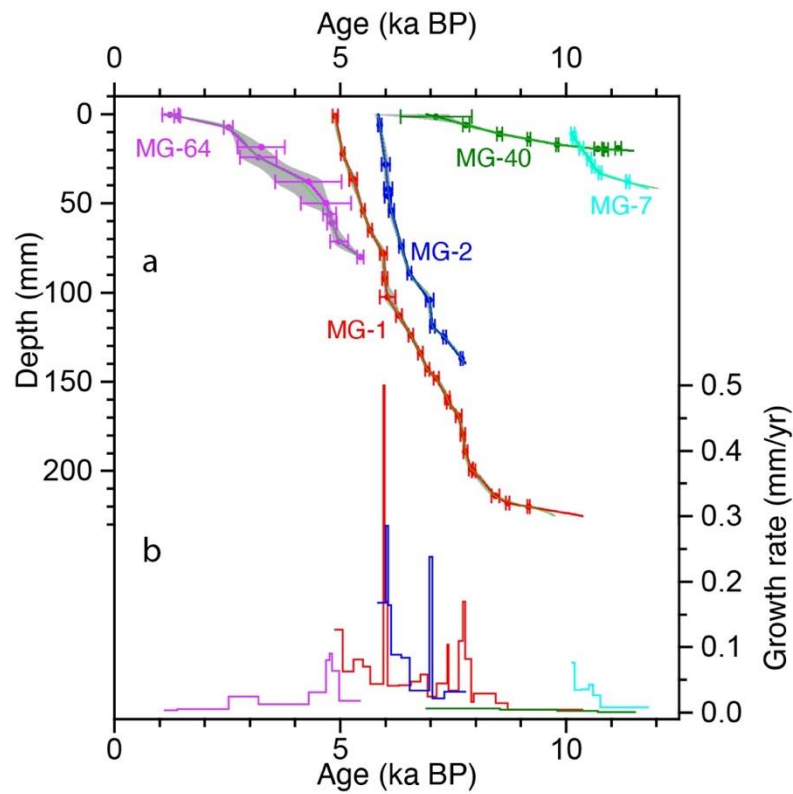943   largely representing the Central Plain of China.

944 Figure 2.
945
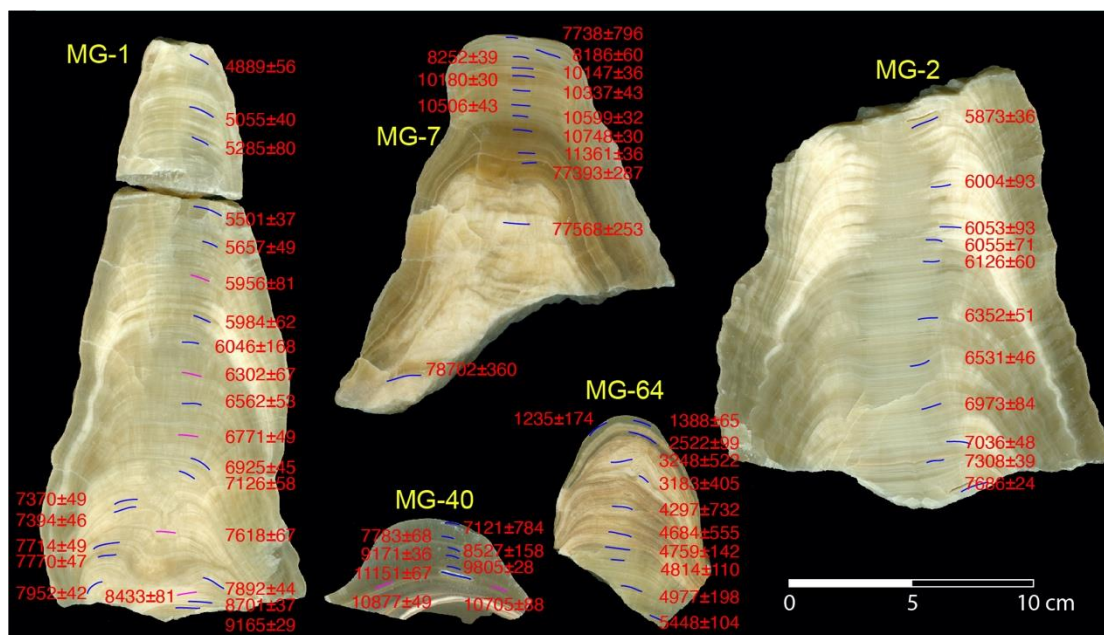
946
947
948 **Figure 2:** Overview with scanned cross-sections of stalagmites MG-1, MG-2, MG-7,

949 MG-40 and MG-64. ^{230}Th dates are indicated in red next to the drilled slits. Drill spots

950 shown in light purple indicate newly taken dating samples added in MG-1 and MG-40

951 in this study.

952 Figure 3.
953

954
955
956 **Figure 3:** Age-depth models (a) and grow rate time series (b) for stalagmites MG-1,

957 MG-2, MG-7, MG-40 and MG-64. All ages of the stalagmites are reported as

958 thousand years before present (1950 AD), ka BP. The indicated age errors are 2σ

959 error. Both the linear interpolation and COPRA pchip models are used to calculate the

960 chronologies of all these stalagmites. The chronological differences between both

961 approaches are negligible because of the high density of dates and relatively small

962 dating errors (most errors are <1%). Different colors denote individual stalagmites.

963

964   Figure 4.
965
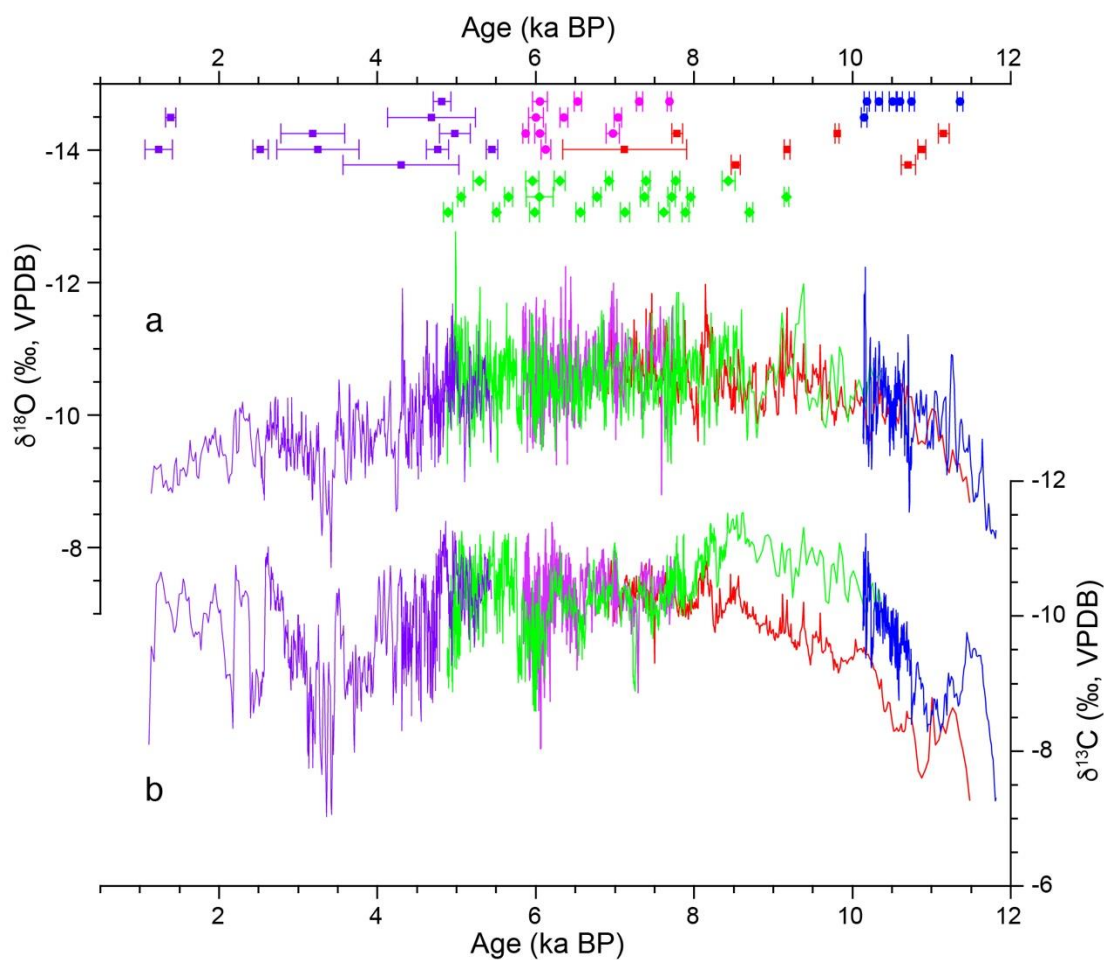
966
967
968   **Figure 4:** The individual time series of speleothem $\delta^{18}O$ (a) and $\delta^{13}C$ (b) obtained

969   from Magou Cave. The ^{230}Th dates are shown with 2σ error. The different stalagmites

970   are color-coded, MG-1 is shown in green; MG-2 in pink; MG-7 in blue; MG-40 in

971   red; and MG-64 in purple.

972

973   Figure 5.

974
975
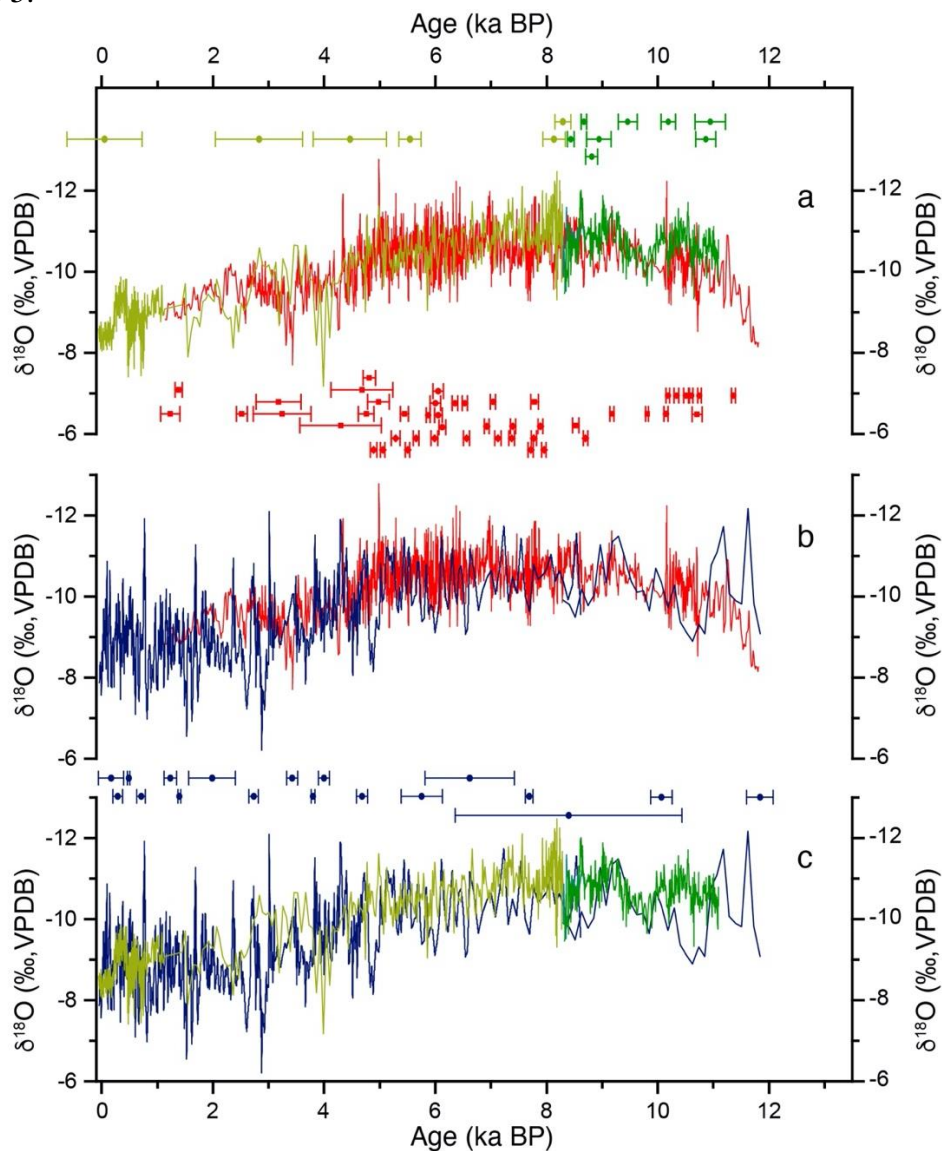
Figure 5: Comparisons of the MG composite δ¹⁸O record and other speleothem δ¹⁸O time

series from central China. a) the MG composite δ¹⁸O record (red, this study) and the δ¹⁸O

record of the Laomudong/Dongshiya Caves (green for Dongshiya Cave and yellow green for

Laomudong Cave, Zhang et al., 2018); b) the MG composite δ¹⁸O record (red, this study) and

the δ¹⁸O record from Jiuxian Cave (blue, Cai et al., 2010); c) the δ¹⁸O records from Jiuxian

Cave (blue, Cai et al., 2010) and the Laomudong/Dongshiya Caves (green for Dongshiya

Cave and yellow green for Laomudong Cave, Zhang et al., 2018). ²³⁰Th dates with 2 σ errors

of each record from different caves are also shown and color-coded by using the same color

as the δ¹⁸O record.
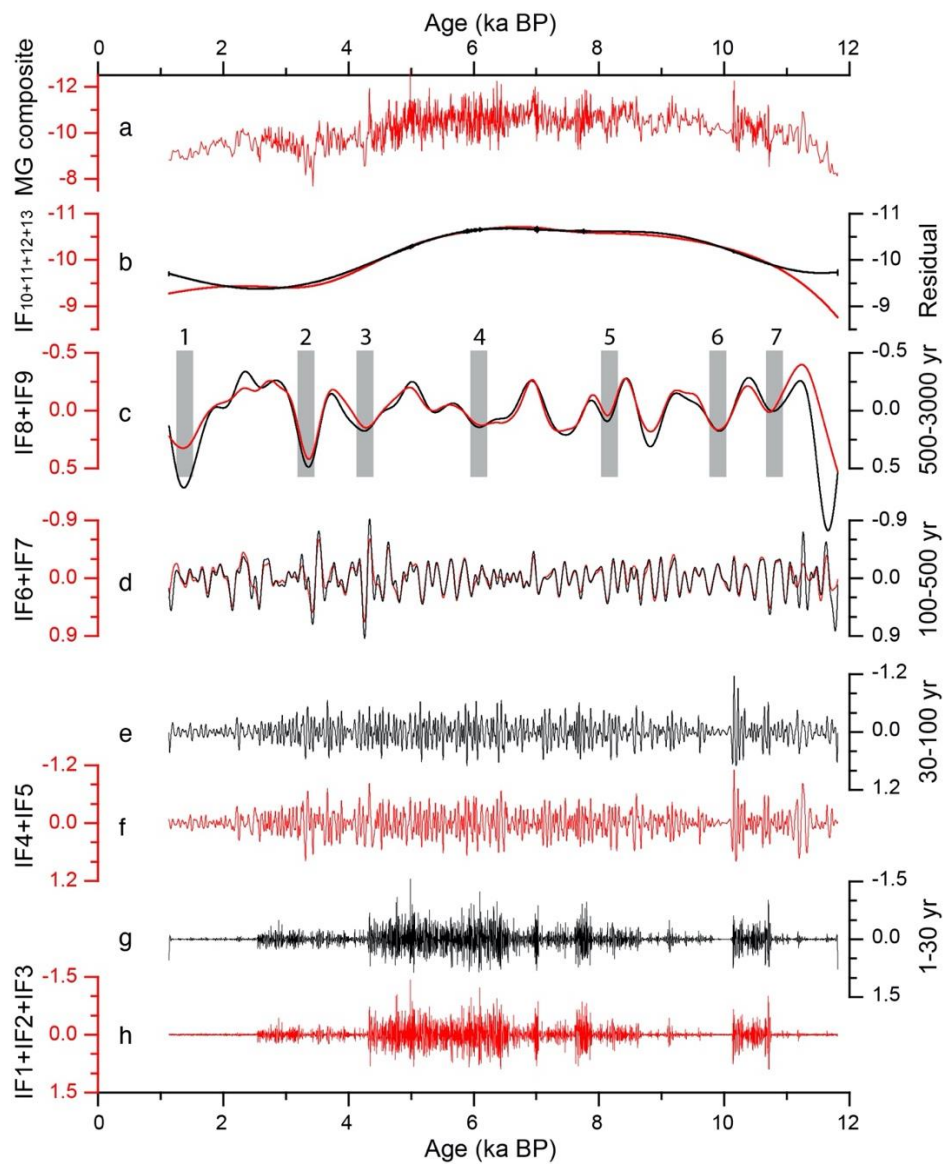
Figure 6: The MG composite time series (a) from ~11.7-1.1 ka BP and derived EEMD

components (red) and wavelet band-pass components (black) (b-h). For the EEMD

decomposition, noise of 0.2 standard deviations of the data is added for the ensemble

calculation, with an ensemble number is 500. Five EEMD components (i.e. sum of

components 1-3, sum of components 4-5, sum of components 6-7, sum of components 8-9,

and sum of components 10-13) are presented. The wavelet band-pass components indicate the

variation of speleothem $\delta^{18}O$ on different timescales and correspond well with the EEMD

components.
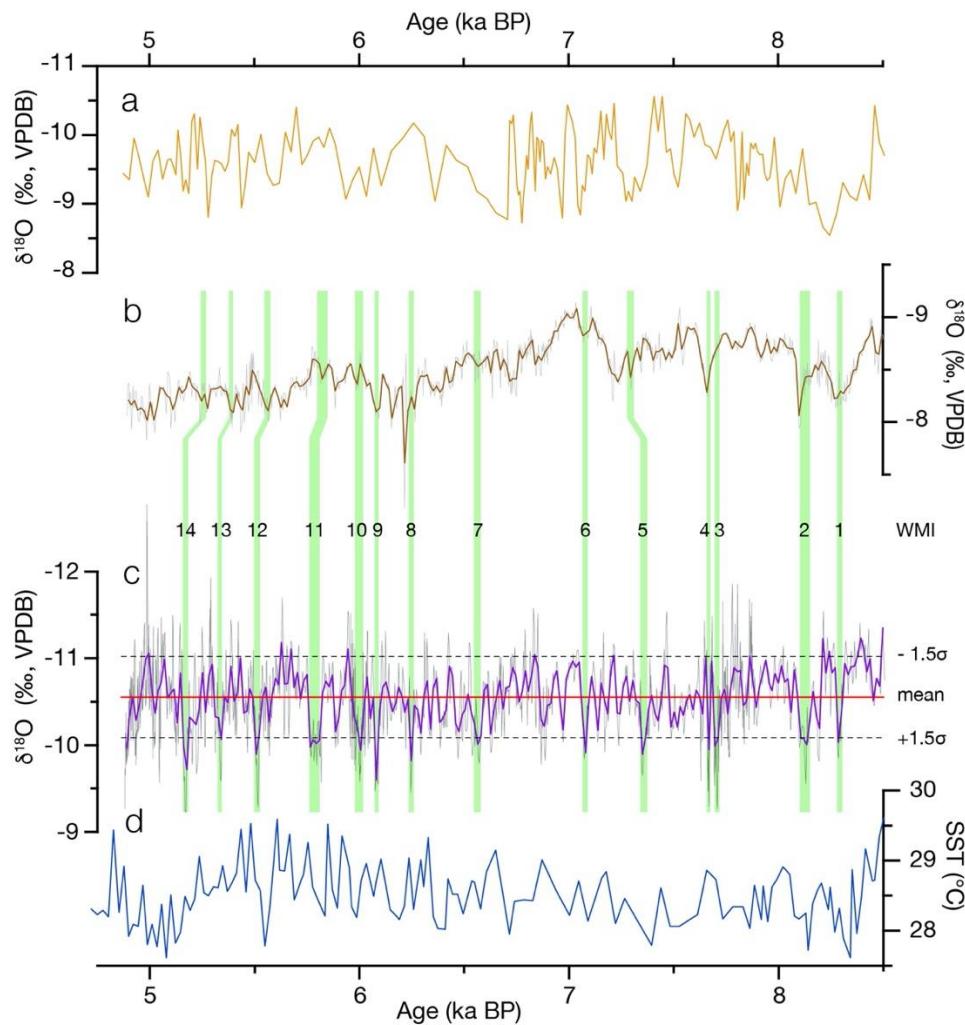
Figure 7: Comparison of speleothem δ^{18}O records and west Pacific warm pool sea surface

temperature (SST) during the Holocene megathermal (8.5 to 4.8 ka BP). a) the speleothem

δ^{18}O record from Heshang Cave; b) the speleothem δ^{18}O record from Dongge Cave. The

brown line represents the 15-year weighted-average time series. c) the speleothem δ^{18}O

record from Magou Cave. The purple line represents the 15-year weighted-average time

series, in which we identify 14 weak summer monsoon intervals (numbered green shades)

using a threshold of ±1.5 standard deviations from the mean δ^{18}O. d) the SST time series

obtained from drill core MD-98-2178 (Fan et al., 2018).

1008   Figure 8.

1009
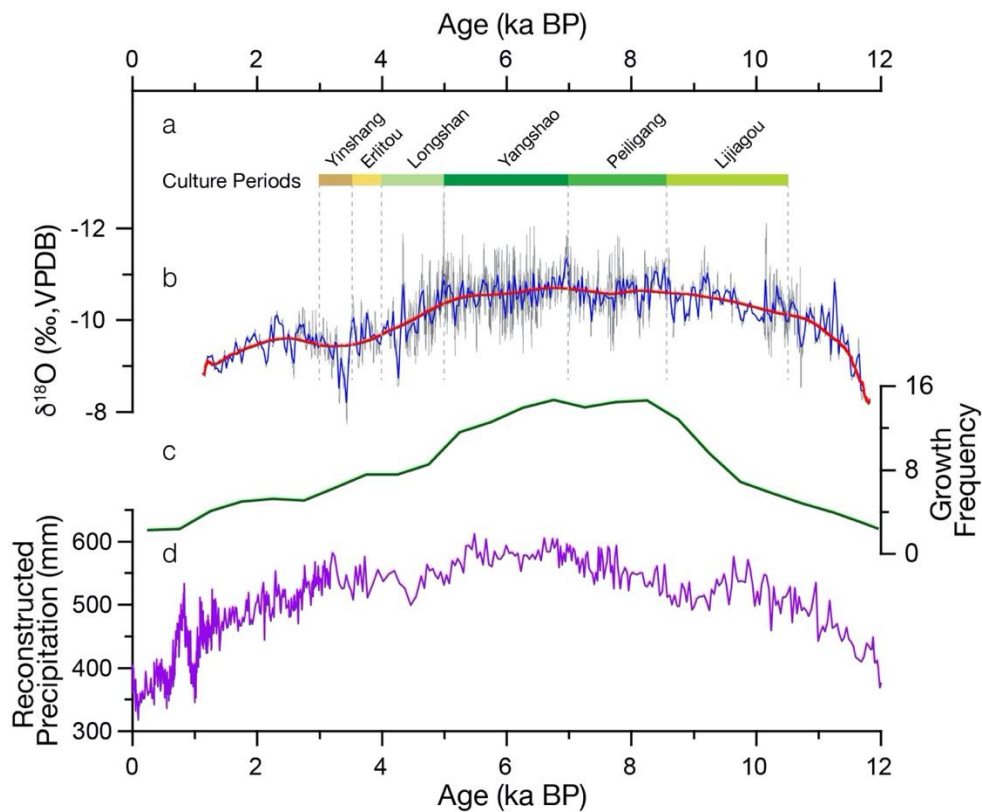
1010
1011
1012   **Figure 8:** The MG composite time series of stalagmite δ¹⁸O (b, this study), the growth

1013   frequency record of Longfeng Cave (c, Wei et al., 2020), the reconstructed precipitation using

1014   the fossil pollen assemblages from Gonghai Lake (d, Chen et al., 2015) and ancient cultural

1015   periods as observed in Henan Province, central China (a, Li et al., 2015a). The grey, blue and

1016   red lines denote the original, 30-years adjacent-averaged and 2000-year weighted-average

1017   curves of MG composite record, respectively. The color bars indicate different archeological

1018   culture periods.